Neurobiology of Disease 130 (2019) 104510

Contents lists available at ScienceDirect

Neurobiology of Disease

journal homepage: www.elsevier.com/locate/ynbdi

Attenuation of epileptogenesis by 2-deoxy-D-glucose is accompanied by increased cerebral glucose supply, microglial activation and reduced astrocytosis

Ina Leiter[a,b,1], Pablo Bascuñana[b], Frank Michael Bengel[b], Jens Peter Bankstahl[b,2], Marion Bankstahl[a,*,2,3]

[a] Department of Pharmacology, Toxicology and Pharmacy, University of Veterinary Medicine Hannover and Center for Systems Neuroscience, Bünteweg 17, 30559 Hannover, Germany
[b] Department of Nuclear Medicine, Hannover Medical School, 30625 Hannover, Germany

ARTICLE INFO

Keywords:
Glucose metabolism
Mouse model
PET imaging
Epilepsy
Microglia

ABSTRACT

Rationale: Neuronal excitability and brain energy homeostasis are strongly interconnected and evidence suggests that both become altered during epileptogenesis. Pharmacologic modulation of cerebral glucose metabolism might therefore exert anti-epileptogenic effects. Here we provide mechanistic insights into effects of the glycolytic inhibitor 2-deoxy-D-glucose (2-DG) on experimental epileptogenesis by longitudinal 2-deoxy-2[^{18}F]fluoro-D-glucose positron emission tomography ([^{18}F]FDG PET) and histology.

Methods: To imitate epileptogenesis, 6 Hz-corneal kindling was performed in male NMRI mice by twice daily electrical stimulation for 21 days. Kindling groups were treated i.p. 1 min after each stimulation with either 250 mg/kg 2-DG (CoKi_2-DG) or saline (CoKi_vehicle). A separate group of unstimulated mice was treated with 2-DG (2-DG_only). Dynamic 60-min [^{18}F]FDG PET/CT scans were acquired at baseline and interictally on days 10 and 17 of kindling. [^{18}F]FDG uptake (%injected dose/cc) was quantified in predefined regions of interest (ROI) using a MRI-based brain atlas, and kinetic modelling was performed to evaluate glucose net influx rate K_i and glucose metabolic rate MR_{Glu}. Furthermore, statistical parametric mapping (SPM) analysis was applied on kinetic brain maps. For histological evaluation, brain sections were stained for glucose transporter 1 (GLUT1), astrocytes, microglia, as well as dying neurons.

Results: Post-stimulation 2-DG treatment attenuated early kindling progression, indicated by a reduction of fully-kindled mice, and a lower overall percentage of type five seizures. While 2-DG treatment alone led to globally increased K_i and MR_{Glu} values at day 17, kindling progression per se did not influence glucose turnover. Kindling accompanied by 2-DG treatment, however, resulted in regionally elevated [^{18}F]FDG uptake as well as increased K_i at days 10 and 17 compared both to baseline and to the 2-DG_only group. In hippocampus and thalamus, higher MR_{Glu} values were found in the CoKi_2-DG vs. the CoKi_vehicle group at day 17. *t* maps resulting from SPM analysis generally confirmed the results of the ROI analysis, and additionally revealed increased MR_{Glu} restricted to the ventral hippocampus when comparing the CoKi_2-DG and the 2-DG_only group both at days 10 and, more distinct, day 17. Immunohistochemical staining showed an attenuated kindling-induced regional activation of astrocytes in the CoKi_2-DG group. Interestingly, 2-DG treatment alone (and also in combination with kindling, but not kindling alone) led to increased microglial activation scores, whereas neither staining of

Abbreviations: BBB, blood-brain barrier; CoKi, corneal kindling; 2-DG, 2-deoxy-D-glucose; 3D-OSEM, three-dimensional ordered subset expectation maximization; [^{18}F]FDG, 2-deoxy-2-[^{18}F]fluoro-D-glucose; GFAP, glial fibrillary acidic protein; GLUT1, glucose transporter 1; IBA1, ionized calcium-binding adapter molecule 1; ID, injected dose; IDIF, image-derived input function; K_i, glucose net influx rate; LC, lumped constant; MAP algorithm, maximum a posteriori algorithm; MR_{Glu}, glucose metabolic rate; PET, positron emission tomography; MRI, magnetic resonance imaging; PET, positron emission tomography; ROI, region of interest; SPM, statistical parametric mapping

* Corresponding author at: University of Veterinary Medicine Hannover, Department of Pharmacology, Toxicology and Pharmacy, Bünteweg 17, D-30559 Hannover, Germany.
E-mail address: bankstahl.marion@mh-hannover.de (M. Bankstahl).
[1] Present address: Institute of Neuroanatomy and Cell Biology, Hannover Medical School, 30625 Hannover, Germany
[2] These authors contributed equally to this study.
[3] Present address: Institute for Laboratory Animal Science and Central Animal Facility, Hannover Medical School, 30625 Hannover, Germany

https://doi.org/10.1016/j.nbd.2019.104510
Received 7 September 2018; Received in revised form 2 June 2019; Accepted 14 June 2019
Available online 15 June 2019
0969-9961/

GLUT1 nor of dying neurons revealed any differences to untreated controls.
Conclusions: Post-stimulation treatment with 2-DG exerts disease-modifying effects in the mouse 6 Hz corneal kindling model. The observed local increase in glucose supply and turnover, the alleviation of astroglial activation and the activation of microglia by 2-DG might contribute separately or in combination to its positive interference with epileptogenesis.

1. Introduction

About 50 million people worldwide are affected by epilepsy, many of them suffering from psychiatric or cognitive comorbidities or pharmacoresistance (WHO, 2018). The mechanisms underlying epileptogenesis are still to be fully explored, and the medical need to develop a treatment interfering with epileptogenesis or modifying its disease progression remains (Baulac et al., 2015; Löscher and Brandt, 2010). Nonetheless, previous and ongoing research has shed further light on cerebral processes following epileptogenic brain insults potentially contributing to epilepsy development. In this regard, preclinical positron emission tomography (PET) studies utilizing the radiotracer 2-deoxy-2-[^{18}F]fluoro-D-glucose ([^{18}F]FDG) demonstrate that changes in brain glucose metabolism can be found during disease development. Whereas a cerebral glucohypermetabolism is described shortly after status epilepticus as epileptogenic brain insult (Kornblum et al., 2000; Mirrione et al., 2006, 2007), glucohypometabolism represents a common finding during subacute and subsequent stages of epileptogenesis as well as during chronic epilepsy (Bascunana et al., 2016; Goffin et al., 2009; Jupp et al., 2012; Lee et al., 2012; Liu et al., 2010; Zhang et al., 2015). This is consistent with the glucohypermetabolism observed in human epilepsy patients while seizing (Struck et al., 2016) and the hypometabolic appearance of epileptic foci in interictal [^{18}F]FDG PET imaging used for pre-surgical evaluation (Burneo et al., 2015; Drzezga et al., 1999). In view of these glucometabolic alterations as a typical feature of epileptogenesis and chronic epilepsy, targeting cerebral energy metabolism during disease development might exert positive influence on later disease outcome.

2-Deoxy-D-glucose (2-DG), a candidate anti-seizure drug under preclinical evaluation (Bialer et al., 2017), impedes the glycolytic pathway (Xi et al., 2014) and represents an eligible compound for influencing cerebral glucose metabolism. After crossing the blood-brain barrier (BBB) via transport by glucose transporter 1 (GLUT 1), penetration into brain cells and transformation to 2-DG-6-phosphate by hexokinase, it cannot be further metabolized and accumulates intracellularly (Kipnis and Cori, 1959). Here, 2-DG-6-phosphate competes with glucose-6-phosphate for phosphoglucose isomerase (Nirenberg and Hogg, 1958; Wick et al., 1957) and seems to inhibit hexokinase non-competitively (Chen and Gueron, 1992).

2-DG exerts acute anticonvulsant effects in several models of chronic epilepsy or acute seizures (Gasior et al., 2010; Lian et al., 2007; Stafstrom et al., 2008, 2009; Yang et al., 2013). Sustained anticonvulsant effects were seen in terms of increased afterdischarge thresholds in the perforant path kindling model in rats (Stafstrom et al., 2009). Beyond this, impeded kindling progression was reported in three rat kindling models (amygdala kindling, perforant path kindling, and olfactory bulb kindling) (Garriga-Canut et al., 2006; Stafstrom et al., 2009). Despite this increasing evidence also for anti-epileptogenic properties of 2-DG, knowledge about its mechanistic basis in the context of epileptogenesis is relatively limited.

Aim of this study was to evaluate the impact of post-stimulation 2-DG treatment on epileptogenesis in the mouse 6 Hz corneal kindling model. Longitudinal [^{18}F]FDG PET was performed to evaluate impact of 2-DG treatment on cerebral glucometabolism during kindling progression, as well as complementary histology to analyse potential involvement of astro- and microglial activation, GLUT1 expression, and neuronal viability.

2. Materials and methods

2.1. Animals

Male NMRI mice from Charles River (Sulzfeld, Germany) were used in all experiments. They were purchased at an age of about six weeks, weighing 30–35 g. Experiments commenced after one week of adaptation during which mice were repetitively handled to get used to experimental procedures. Animals were housed in groups of 9 animals in individually ventilated cages (Allentown, Neuss, Germany) with bedding and nesting material, under constant laboratory conditions: 20–22 °C, air humidity of 45–55%, 14 h light phase (7 am to 9 pm) and 10 h dark phase. Autoclaved water and a standard rodent diet (Altromin, Lage, Germany) were offered ad libitum. Any efforts were made to diminish suffering of the experimental animals at the best. All experiments were performed in conformity with the EU directive 86/609/EWG and the German animal welfare act, with the permission of the Lower Saxony State Office for Consumer Protection and Food Safety (LAVES). Experiments were planned and reported according to ARRIVE (Animal Research: Reporting in Vivo Experiments) guidelines (Kilkenny et al., 2010).

2.2. Drugs

For the intraperitoneal (i.p.) injections, 250 mg/kg 2-DG (Sigma-Aldrich, Steinheim, Germany) were freshly dissolved in 10 ml/kg 0.9% sterile saline. Vehicle-treated animals received i.p. injections of 10 ml/kg 0.9% sterile saline. Tetracaine hydrochloride (Sigma-Aldrich) was dissolved in *aqua ad injectabilia* to produce a 2% tetracaine eye drops solution.

2.3. Animal groups and treatment

The experimental design is provided in Fig. 1. Mice were randomized to the experimental groups. During the experiment, two groups of mice were kindled: A 2-DG-treated group (CoKi_2-DG, $n = 18$), injected i.p. with 250 mg/kg 2-DG 1 min after each stimulation, and a vehicle-treated group (CoKi_vehicle, n = 18) receiving i.p. injections of saline 1 min after each stimulation. An additional group of mice was not stimulated, but was injected with 250 mg/kg 2-DG i.p. at the same time points as the animals undergoing kindling (2-DG_only, $n = 12$). A group of age-matched naïve mice kept under the same conditions ($n = 6$) served as reference group for histological analyses. The last treatment or stimulation before each PET scanning was performed the evening before, i.e. 18–20 h prior [^{18}F]FDG PET, to avoid acute effects of 2-DG or stimulation. The next kindling stimulation and treatment were resumed the evening after PET scanning. Drug or vehicle treatment began on the evening before the first PET scan (without stimulation). Through this, the drug treatment state of mice was hold as comparable as possible for all acquired [^{18}F]FDG PET scans. Further, this allowed intergroup comparison of baseline data for assessing potential effects of 2-DG treatment on brain glucose metabolism that might have persisted even after the 18–20 h time interval between injection and [^{18}F]FDG PET.

2.4. Corneal kindling

A stimulator (ECT UNIT, 57800, Ugo Basile, Comerio, Italy) with

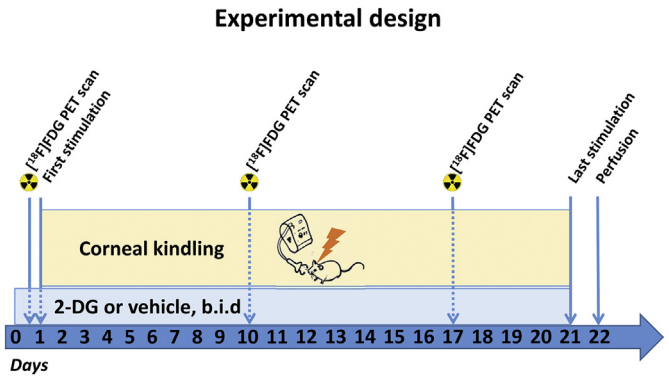

Fig. 1. Experimental design.
On the evening before the first [^{18}F]FDG PET scan (baseline scan, day 0) treatment with either 2-DG (250 mg/kg twice daily; $n = 18$) or vehicle ($n = 18$) was started. 6 Hz corneal kindling was started on the evening of day 1 and consisted of twice daily stimulations until day 21. A second and third [^{18}F]FDG PET scan were performed on days 10 and 17 of ongoing kindling procedure, always before the first 2-DG or vehicle injection of the respective day. On day 22, mice were transcardially perfused and brains harvested for histological analyses. A third group of mice ($n = 12$) receiving 2-DG treatment and undergoing PET scans remained unstimulated.

leather-covered corneal electrodes (soaked in 0.9% saline) was used to deliver the corneal kindling stimuli twice daily for 21 days. The stimuli were monopolar, lasted for 3 s, had a frequency of 6 Hz, a current intensity of 44 mA, and a pulse duration of 0.2 ms (Leclercq et al., 2014). The inter-stimulation interval was at least 6 h. Two minutes prior to stimulation, a drop of the tetracaine solution was added to both eyes of each individual animal. A stopwatch was used to ensure the appropriate time period for induction of local anaesthesia. During stimulation, the animals were manually restrained. Immediately afterwards, the mice were unclasped and closely observed for the expression of motor seizures within the first minute after stimulation. The seizure duration was recorded and seizure severity was scored using a modified Racine scale (Racine, 1972): score 0, immobility or no reaction; score 1, mild facial clonus: eye blinking/closing, twitching of the vibrissae, stereotyped sniffing; score 2, severe facial clonus: chewing, head nodding, and/or myoclonic twitches of the forelimbs; score 3, clonic convulsions of one forelimb without rearing; score 4, clonic convulsions of both forelimbs with/without rearing; score 5, generalized clonic convulsions with immediate loss of balance (also in lateral position); score 6, tonic seizure of fore- and hind limbs. Mice showing at least eight stage five seizures within ten consecutive stimulations were declared fully kindled. Body weight was determined each day in order to deliver the appropriate treatment dosage and to control the health status of the animals. The first corneal kindling stimulation was done in the evening after the first [^{18}F]FDG PET scan.

2.5. Image acquisition

A dedicated small animal PET-CT scanner was used for imaging brain glucose turnover (Inveon DPET, Siemens, Knoxville, TN, USA). Mice were scanned at three time points: At day 1 (baseline), i.e. after first 2-DG or vehicle treatment but before first kindling stimulation, at day 10, and at day 17 of kindling. Anaesthesia induction was performed with 3% isoflurane in 3 l/min oxygen. During the scanning procedure, the isoflurane concentration was adapted (about 1–1.5% in 0.6 l/min) to each animal to maintain a respiration frequency of about 60–80/min. Prior to tracer injection, blood glucose was measured from the vena saphena (Contour NEXT meter, Bayer, Germany). Animals were then placed side-by-side in a double mouse scan bed (Minerve, Esternay, France). During anaesthesia, respiration frequency was monitored and bed temperature was maintained at 37 °C. The head of the mice was positioned in the center field of view. The tracer (8.38 ± 0.46 MBq (mean ± SD) [^{18}F]FDG in a volume of 0.15 ml) was injected into a lateral tail vein and dynamic acquisitions of 60 min were obtained starting with tracer injection. The acquired list mode data were histogrammed to 32 frames. The image reconstruction to a 128 × 128 × 159 matrix (0.78 × 0.78 × 0.8 mm^3) was done with a three-dimensional ordered subset expectation maximization (3D-OSEM)/maximum a posteriori (MAP) algorithm ($\beta = 1$, OSEM iterations = 2, MAP iterations = 18) with scanner-applied scatter correction. Attenuation was corrected using a ^{57}Co transmission scan. After each [^{18}F]FDG PET scan, a standard CT acquisition followed for anatomical co-registration. After the scanning procedure, blood glucose levels were measured again from the tail vein after removal of the catheter. Average total duration of anaesthesia was 114.9 ± 9.56 min (mean ± SD).

2.6. Image data processing and kinetic modelling

Image data were processed using PMOD 3.6 software (PMOD Technologies, Switzerland). First, each CT image was co-registered to the standard mouse MRI atlas of PMOD (T_2-weighted, (Ma et al., 2005)). Second, each CT image was co-registered to the correlating PET image, resulting in an exact overlap of MRI atlas and PET image. As a reliable standard approach, the [^{18}F]FDG uptake was analyzed in selected ROIs (hippocampus, thalamus, amygdala, cortex, striatum, cerebellum) which were located using the volumetric ROI mouse brain atlas provided in this PMOD version. This ROI atlas was originally generated and further validated by Mirrione et al. (2007) from overlaying a standard T2-weighted MRI mouse brain template from Ma et al. (2005) with the stereotaxic mouse brain atlas from Paxinos and Franklin (2001). The tracer uptake values of the analyzed brain regions were calculated from the last two frames (i. e. the last 20 min of the acquisition) and expressed as percent injected dose per cubic centimeter. The kinetic modelling was performed using the FDG two-tissue compartment model offered in the PMOD kinetic modelling tool. For this, an image-derived input function (IDIF) was obtained by calculation of the whole blood time-activity-curve for a region of interest (2 × 2 × 4 mm^3) positioned in the early frame images on the vena cava caudalis (Lanz et al., 2014; Thorn et al., 2013). The used lumped constant LC (which delineates the different properties of glucose and [^{18}F]FDG concerning the uptake and the phosphorylation) was 0.67 (Thorn et al., 2013). Individual blood glucose values of both measurements (before and after each scan) were averaged and then introduced in the modelling process.

2.7. Statistical parametric mapping analysis

[^{18}F]FDG images underwent voxel-based kinetic modelling applying the Patlak model in the Pxmod module (Pmod software) and the K_i and MR_{Glu} parametric images were calculated. For whole-brain voxel wise intra- and intergroup comparisons, SPM12 software (SPM; Wellcome Trust Center for Neuroimaging, UCL, London, UK) was used in MATLAB (TheMathWorks, Natick, Ma, USA). [^{18}F]FDG K_i and MR_{Glu} parametric images of the different groups at the three time points were compared by a two-sample unpaired *t*-test. A significance level threshold of 0.05 (uncorrected for multiple comparisons) and a minimum cluster size of 10 voxels was selected. Parametric *t* maps resulting from each comparison were loaded in PMOD and fused to the T2-MRI template (Ma et al., 2005). The *t*-value threshold was set individually for each time point to show voxels with a correspondent *p* value lower than 0.05. Anatomical localization of intra- and intergroup differences identified by SPM analysis was defined by thorough visual inspection of the *t* maps fused to the reference MRI mouse brain atlas integrated in PMOD (Mirrione et al., 2007) as exemplary illustrated each on one coronal and one horizontal section of the MRI template in Fig. 4E.

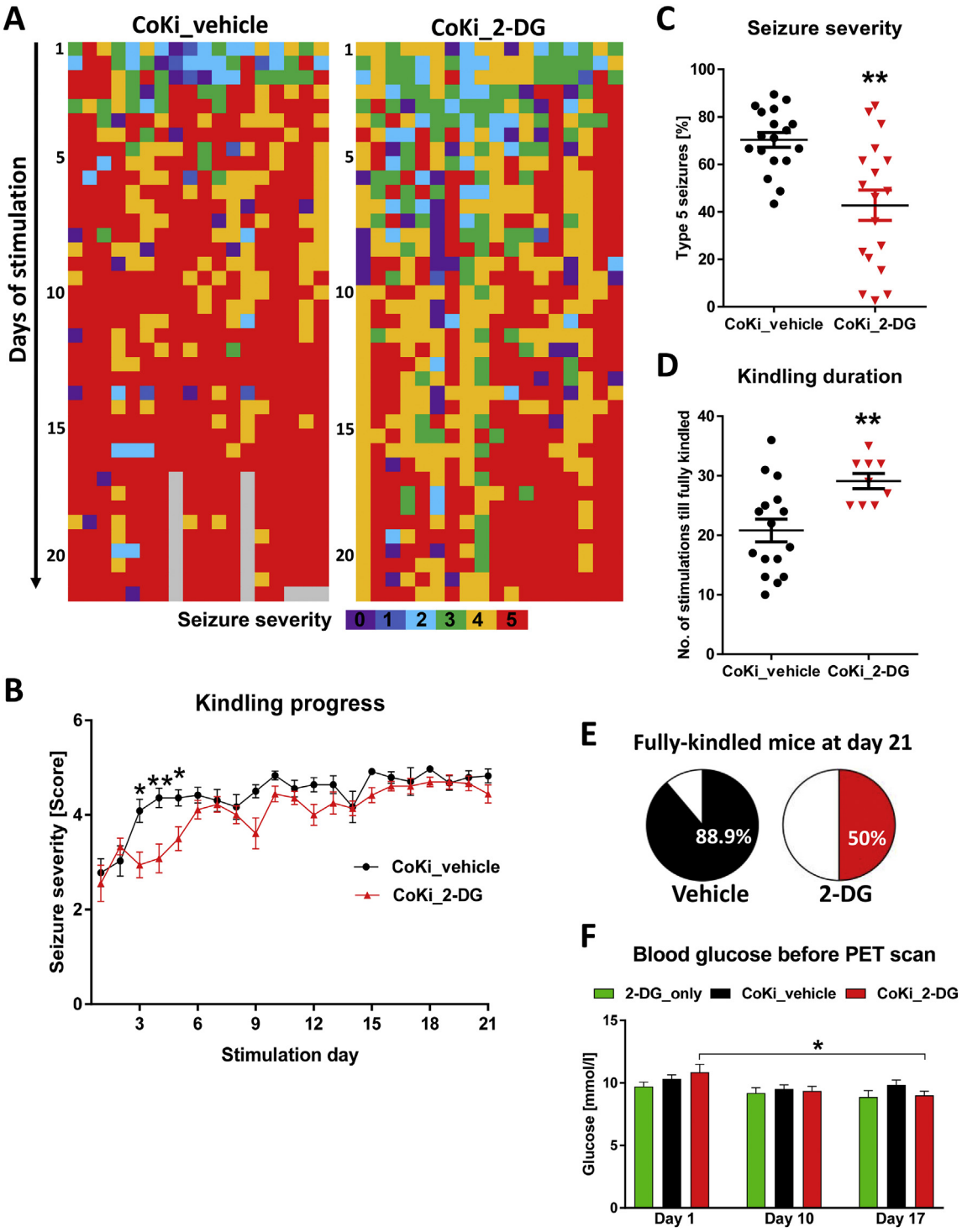

Fig. 2. Effects of 2-deoxy-D-glucose (2-DG) treatment on 6 Hz corneal kindling.
(A) Heat map (purple to red) indicating seizure responses to each stimulation in mice treated with vehicle (left, CoKi_vehicle, n = 18) or 2-DG (right, CoKi_2-DG, n = 18) 1 min after each stimulation (twice daily). (B) Seizure responses of vehicle- and 2-DG-treated mice over the kindling course of 21 days. (C) Percentage of overall shown type-5 seizures relative to all stimulations per individual animal in vehicle- and 2-DG-treated mice. (D) Number of stimulations needed to achieve a fully kindled state, defined as at least 8 of 10 consecutive type 5 seizures, in vehicle- and 2-DG-treated mice. (E) Percentage of fully-kindled mice on stimulation day 21. (F) Blood glucose levels measured before each PET scan in unstimulated mice treated with 2-DG, as well as kindled mice treated with vehicle or 2-DG. Mean ± SEM; Kruskal-Wallis ANOVA, Dunn's multiple comparison post-hoc test (B), Student's *t*-test (C, D), Fisher's exact-test (E), repeated-measures one-way ANOVA, Dunnett's multiple comparison test (F); $p < .05$. Asterisk indicates significant difference between treatment groups. (For interpretation of the references to colour in this figure legend, the reader is referred to the web version of this article.)

2.8. Immunohistochemical staining and analysis of astroglial and microglial activation

On day 22 after start of kindling, mice were deeply anaesthetized using ketamine and xylazine. They were trans-cardially perfused with 25 ml 0.01 M phosphate-buffered saline and thereafter with 25 ml 4% paraformaldehyde solution (dissolved in 0.1 M phosphate buffer, pH = 7.4). Brains were removed, transferred into 4% paraformaldehyde solution for 24 h and stored in a solution of 30% sucrose and 0.2% sodium azide in 0.1 M phosphate buffer until slicing. Brains of the age-matched naïve controls and of 6 randomly chosen mice per treatment group were sliced on a sliding microtome (Frigomobil CM 1325, Leica, Wetzlar). Slices (40 µm thickness) were stored in 0.1 M phosphate buffered saline until used for immunohistochemical staining (free-floating method). Rabbit anti-mouse glucose transporter 1 (GLUT1) antibody (1:1000; Biotrend Chemikalien GmbH, Cologne, Germany) was used as primary antibody. Endogenous peroxidase activity was inhibited using 0.5% hydrogen peroxide. Unspecific antibody binding sites were blocked with 10% donkey serum. Slices were incubated for 20 h in the primary antibody solution at 7 °C. Slices were exposed to the secondary antibody (biotin-SP-conjugated affinipure donkey anti-rabbit IgG, 1:500; Jackson ImmunoResearch Laboratories Europe, Suffolk, UK) for 1 h at room temperature. Vectastain ABC kit (Burlingame, CA, USA) provided the avidin-biotin complex for the final visualization reaction with 3,3′-diaminobenzidine solution and hydrogen peroxide. Stainings of microglia and astrocytes were performed according to a similar protocol varying in the following steps: Endogenous peroxidase activity was inhibited using 0.6% hydrogen peroxide and the blocking step was done using 5% normal goat serum. Brain slices were exposed to the primary antibody, anti-ionized calcium-binding adapter molecule 1 (IBA1) antibody (1:500; Synaptic Systems, Göttingen, Germany) or the anti-glial fibrillary acidic protein (GFAP) antibody (1:5000; Dako Deutschland GmbH, Hamburg, Germany) for 18 h at room temperature. Peroxidase affinipure goat anti-rabbit IgG (1:500; Jackson ImmunoResearch Laboratories Europe, Suffolk, UK) was used as secondary antibody. Slices were mounted on glass slides (Menzel-Gläser, Thermo Scientific, Braunschweig, Germany) and cover-slipped with mounting medium (Entellan, Merck, Darmstadt, Germany).

GLUT1-stained sections of the four groups were visually inspected in a blinded fashion using a light microscope and screened for group differences in staining intensity in the regions of interest mentioned below. Microglial (IBA1) and astroglial (GFAP) activation was semi-quantitatively scored in a blinded fashion as recently described (Brackhan et al., 2016); score 0 = inactive cells, < 10% activated, score 1 = predominantly inactive cells, about 30% activated, score 2 = some inactive cells, about 60% activated, score 3 = > 90% activated cells). At section levels −1.94 mm and −3.16/−3.28 mm relative to bregma (Paxinos and Franklin, 2001), the following brain regions were assessed: hippocampal cornu ammonis (CA)1, CA3a, and dentate hilus, as well as thalamus, amygdala, piriform and entorhinal cortex (Fig. 5E). Microglial and astroglial scores were each averaged for the two assessed brain section levels. In addition to this rank scale approach, we applied cell counting and morphological assessment on IBA1-stained brain sections based on a recently published methodoligical approach in a rat post-status epilepticus model (Wyatt-Johnson et al., 2017). On section level –1.94 mm, microscopic photographs were bilaterally taken at 400× magnification in a predefined position of each scored brain subregion. Within each image, all IBA1-positive cells were counted and assigned to a certain morphological category (ramified, hypertrophic, bushy, amoeboid, and rod) based on overall cell diameter including processes and appearance of processes each cell (Wyatt-Johnson et al., 2017). As the photograph of the dentate hilus also covered adjacent areas, the actual dentate hilus area within the image frame was measured and only cells in this area were counted and categorized. AxioVision software was used for measurements and counting. Data from both hemispheres were averaged and are presented as IBA1-positive cells per mm^2.

To visualize neurodegeneration, Fluoro-Jade C staining was performed as described before (Gröticke et al., 2007). Briefly, brain slices were mounted on protein glycerol coated glass slides and air-dried. Directly before staining, the slides were bathed twice in ethanol (80%, 5 min, and 70%, 2 min) and in distilled water to remove the latter. Staining was performed with 0.0001% Fluoro-Jade C solution (Merck, Darmstadt, Germany) for 30 min. Slices were cover-slipped with mounting medium (DPX mountant for histology, Sigma-Aldrich). The stained slices (−1.94 mm relative to bregma) were microscopically screened for fluorescence-positive neurons concerning the target regions described above. Brain slices of a mouse intrahippocampally injected with kainic acid served as positive control.

2.9. Statistical analysis

All statistical tests were calculated using GraphPad Prism version 7.00 for Windows (GraphPad Software, San Diego California USA). For comparison of only two data sets (seizure severity, kindling duration) a Student's *t*-test or Fisher's exact test (proportion comparison of fully-kindled mice) was used. Inter-group differences concerning seizure response during kindling progression and histological evaluation were analyzed performing a Kruskal-Wallis analysis of variance (ANOVA) followed by Dunn's Multiple Comparison Test. For intergroup comparison of data gained from counting and morphological microglia assessment ordinary one-way ANOVA followed by Dunnett's multiple comparisons were performed. One-way ANOVA with Bonferroni post tests was conducted regarding the inter-group comparisons of all PET imaging data and repeated-measures one-way ANOVA with Bonferroni post tests was used concerning intra-group comparisons of imaging data. For analysis of blood glucose levels, intra-group comparisons were performed with repeated-measures one-way ANOVA followed by Dunnett's multiple comparison test. If not stated otherwise, data is presented as mean values with standard error of the mean (SEM).

3. Results

3.1. Corneal kindling and tolerability of chronic 2-DG treatment

The 6 Hz corneal kindling course started with seizure responses of type two to three in most animals (Fig. 2A). On days three, four and five of kindling, the 2-DG-treated animals showed significantly attenuated seizure responses ($p < .05$; Fig. 2B). On days eight and nine, the duration of the seizure response was shorter in the 2-DG treated group (13.67 ± 0.7346 vs. 10.17 ± 1.147, $p = .0132$, CoKi_vehicle vs. CoKi_2-DG, day 8, and 14.35 ± 0.8572 vs. 11.64 ± 0.8994, $p = .0383$, CoKi_vehicle vs. CoKi_2-DG, day 9). Over the course of the kindling process, the percentage of type-5 seizures relative to all stimulations per individual was lower in 2-DG-treated than in vehicle-treated mice ($p = .0004$; Fig. 2C). According to the used definition of a fully-kindled state, the percentage of completely kindled mice per group after 39 stimulations was 88.9% in the CoKi_vehicle group and 50% in the CoKi_2-DG group ($p = .0275$, Fig. 2E). The mean number of stimulations needed to achieve a fully-kindled state was increased by 2-DG treatment (20.81 vs. 29.11 stimulations, CoKi_vehicle vs. CoKi_2-DG, $p = .0058$; Fig. 2D). No mortality occurred during corneal kindling. However, five mice had to be killed before end of kindling due to recurrent penis prolapse of unknown origin (Fig. 2A, indicated in grey). Body weight of corneally-kindled mice remained stable over time (day 1 vs. day 21, CoKi_vehicle: 34.36 ± 0.4576 vs. 33.98 ± 0.4784 g, $p = .5761$; CoKi_2-DG: 34.46 ± 0.4961 vs. 33.41 ± 0.5332 g, $p = .1607$), and the mean body weight did not differ between kindled groups at any investigated time point (not shown). Unstimulated mice treated with 2-DG gained about 3 g of body weight over the treatment period of 21 days (day 1 vs. day 21, 35.77 ± 0.5245 vs. 38.58 ± 0.5371 g, $p = .0045$). At the chosen 2-DG dosage (250 mg/kg

twice daily), we did neither observe behavioural abnormalities nor other obvious systemic side effects during twice daily handling and observation of mice.

Blood glucose levels measured directly before each PET scan remained stable in the 2-DG_only and CoKi_vehicle groups compared to individual baseline values, while reduced blood glucose levels were found on day 17 in the CoKi_2-DG group (p = .0221; Fig. 2F).

3.2. Imaging

The 2-DG_only group showed a reduced [^{18}F]FDG uptake on day 17 compared to baseline in thalamus (p = .0372), amygdala (p = .0002), cortex (p = .0243), and striatum (p = .0023; Table 1). While tracer uptake did not change in CoKi_vehicle mice (Table 1), an increased [^{18}F]FDG uptake was detected in CoKi_2-DG mice on day 10 in thalamus (p = .0215) and cerebellum (p = .0042; Table 1). On day 10 of treatment, a higher [^{18}F]FDG uptake was seen in CoKi_2-DG versus 2-DG_only mice in all analyzed brain regions except for the amygdala (hippocampus, p = .0016; thalamus, p = .0293; cortex, p = .0107; striatum, p = .0381; cerebellum, p = .0208; Table 1), whereas on day 17 this was found in hippocampus (p = .0073), amygdala (p = .0012) and striatum (p = .0060; Table 1).

The influx rate K_i as well as the metabolic rate MR_{Glu} was elevated in the 2-DG_only group on day 17 compared to baseline in all analyzed brain regions apart from amygdala (hippocampus, p = .0026; thalamus, p = .0010; cortex, p = .0019; striatum, p = .0060; cerebellum, p = .0037; Table 1; hippocampus, p = .0320; thalamus, p = .0072; cortex, p = .0056; striatum, p = .0137; cerebellum, p = .0169; Table 1). Compared to baseline, kindling alone did neither alter K_i nor MR_{Glu} (Table 1). Nevertheless, MR_{Glu} was higher in hippocampus

Table 1

(A) Quantification of the spatiotemporal profile of [^{18}F]FDG uptake. 2-deoxy-D-glucose (2-DG)-treated, unstimulated mice (2-DG_only, n = 12), vehicle-treated mice undergoing kindling (CoKi_vehicle, n = 18), and 2-DG- treated mice undergoing kindling (CoKi_2-DG, n = 18) were subjected to [^{18}F]FDG PET at baseline (after first treatment, before start of kindling) and at days 10 and 17 of kindling. Regional [^{18}F]FDG uptake in hippocampus, thalamus, amygdala, cortex, striatum and cerebellum, was quantified as percent injected dose per cubic centimeter (%ID/cc). (B) Regional glucose net influx rate (K_i) values derived from the [^{18}F]FDG two-tissue compartment model. The input function for the two-tissue compartment model was calculated from the image data by positioning a volume of interest in the caudal vena cava. (C) Regional glucose metabolic rate (MR_{Glu}) values derived from the [^{18}F]FDG two-tissue compartment model. The input function for the two-tissue compartment model was calculated from the image data by positioning a volume of interest in the caudal vena cava. Data is given as mean ± SEM; one-way ANOVA, Bonferroni post hoc test; $p < .05$. Asterisk indicates significant difference between indicated pairs; sharp indicates significant difference to baseline.

A

[^{18}F]FDG uptake [%ID/cc]		Hippocampus		Thalamus		Amygdala		Cortex		Striatum		Cerebellum	
Baseline	2-DG_only	3.68 ± 0.12		4.10 ± 0.15		2.54 ± 0.10		3.34 ± 0.11		3.75 ± 0.14		4.53 ± 0.16	
	CoKi_vehicle	3.67 ± 0.17		3.96 ± 0.19		2.63 ± 0.13		3.32 ± 0.15		3.72 ± 0.17		4.42 ± 0.25	
	CoKi_2-DG	3.95 ± 0.14		4.15 ± 0.14		2.94 ± 0.13		3.61 ± 0.12		4.02 ± 0.14		4.51 ± 0.15	
10 days	2-DG_only	3.36 ± 0.17		3.87 ± 0.17		2.45 ± 0.10		3.11 ± 0.12		3.51 ± 0.15		4.21 ± 0.18	
	CoKi_vehicle	3.97 ± 0.16	**	4.28 ± 0.17	*	2.68 ± 0.11		3.52 ± 0.13	*	3.79 ± 0.14	*	4.82 ± 0.22	*
	CoKi_2-DG	4.35 ± 0.19		4.65 ± 0.22	#	2.86 ± 0.12		3.76 ± 0.16		4.14 ± 0.19		5.20 ± 0.26	##
17 days	2-DG_only	3.34 ± 0.16		3.75 ± 0.18	#	2.08 ± 0.10	###	3.04 ± 0.13	#	3.31 ± 0.15	##	4.18 ± 0.20	
	CoKi_vehicle	3.68 ± 0.15	**	3.99 ± 0.16		2.52 ± 0.10	**	3.31 ± 0.13		3.68 ± 0.11	**	4.72 ± 0.22	
	CoKi_2-DG	4.11 ± 0.17		4.40 ± 0.19		2.66 ± 0.10		3.51 ± 0.13		3.93 ± 0.13		4.89 ± 0.22	

B

K_i [ml/ml{tissue}/min]		Hippocampus		Thalamus		Amygdala		Cortex		Striatum		Cerebellum	
Baseline	2-DG_only	0.013 ± 0.001		0.016 ± 0.001		0.010 ± 0.000		0.012 ± 0.001		0.013 ± 0.001		0.018 ± 0.001	
	CoKi_vehicle	0.017 ± 0.001		0.019 ± 0.001		0.013 ± 0.001		0.014 ± 0.001		0.017 ± 0.001		0.022 ± 0.002	
	CoKi_2-DG	0.016 ± 0.001		0.017 ± 0.001		0.012 ± 0.001		0.014 ± 0.001		0.016 ± 0.001		0.020 ± 0.001	
10 days	2-DG_only	0.014 ± 0.001		0.016 ± 0.001		0.010 ± 0.001		0.011 ± 0.001		0.013 ± 0.001		0.018 ±0.001	
	CoKi_vehicle	0.019 ± 0.002	*	0.021 ± 0.002	*	0.014 ± 0.001	*	0.015 ± 0.001	*	0.017 ± 0.001	*	0.024 ± 0.002	*
	CoKi_2-DG	0.021 ± 0.002	##	0.023 ± 0.002	###	0.015 ± 0.001	##	0.017 ± 0.002		0.019 ± 0.002	#	0.026 ± 0.002	#
17 days	2-DG_only	0.017 ± 0.001	##	0.020 ± 0.001	##	0.011 ± 0.001		0.015 ± 0.001	##	0.016 ± 0.001	##	0.023 ± 0.001	##
	CoKi_vehicle	0.018 ± 0.001		0.020 ± 0.001		0.012 ± 0.001	*	0.015 ± 0.001		0.016 ± 0.001		0.024 ± 0.002	
	CoKi_2-DG	0.022 ± 0.002	###	0.024 ± 0.002	###	0.015 ± 0.001	###	0.017 ± 0.001		0.020 ± 0.002	##	0.027 ± 0.002	###

C

MR_{Glu} [mmol/min/g]		Hippocampus		Thalamus		Amygdala		Cortex		Striatum		Cerebellum	
Baseline	2-DG_only	20.44 ± 1.34		23.97 ± 1.58		14.86 ± 0.71		17.84 ± 1.24		20.47 ± 1.43		27.73 ± 2.40	
	CoKi_vehicle	24.75 ± 1.96		28.15 ± 1.82		19.38 ± 1.45		21.42 ± 1.89		25.66 ± 2.02		32.00 ± 2.03	
	CoKi_2-DG	28.21 ± 3.17		30.64 ± 2.92		21.36 ± 2.06		24.00 ± 2.65		28.27 ± 2.94		34.74 ± 2.92	
10 days	2-DG_only	21.67 ± 1.11		26.31 ± 1.30		16.42 ± 0.78		18.61 ± 0.90		22.31 ± 1.20		29.92 ± 1.47	
	CoKi_vehicle	23.24 ± 3.17		27.39 ± 2.99		18.40 ± 2.40		19.83 ± 2.22		24.11 ± 2.66		31.28 ± 2.44	
	CoKi_2-DG	27.87 ± 2.97		31.43 ± 2.85		20.31 ± 1.63		22.71 ± 2.23		26.78 ± 2.37		35.13 ± 3.20	
17 days	2-DG_only	23.70 ± 1.37	#	29.09 ± 1.94	##	15.94 ± 0.93		21.57 ± 1.30	##	24.73 ± 1.86	#	33.49 ± 2.18	#
	CoKi_vehicle	20.90 ± 1.90	*	25.07 ± 1.99	*	15.90 ± 1.36		18.41 ± 1.56		21.67 ± 1.85		30.44 ± 2.09	
	CoKi_2-DG	29.09 ± 2.56		33.49 ± 2.58		20.89 ± 1.71		23.66 ± 1.94		28.54 ± 2.21		37.39 ± 2.75	

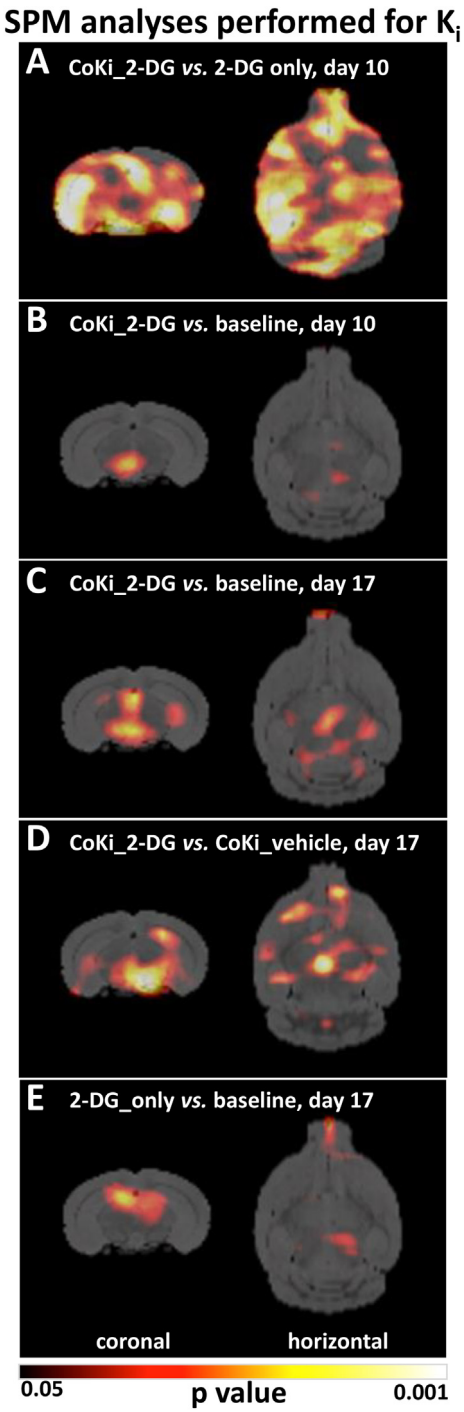

Fig. 3. Statistical parametric mapping (SPM) analysis of [^{18}F]FDG K_i maps in mice undergoing 2-deoxy-D-glucose (2-DG) treatment in combination with or without corneal kindling (CoKi).
Coronal (~3.1 mm caudal to bregma; left), and horizontal (~1.5 mm ventral to bregma; right) *t* maps resulting from voxel wise comparisons (Student's *t*-test) of [^{18}F]FDG K_i maps are shown for comparison of (A) 2-DG-treated mice with and without kindling on day 10, (B, C) 2-DG-treated, kindled mice on experimental days 10 and 17 compared to baseline, (D) 2-DG-treated versus vehicle-treated kindled mice on day 17, and (E) 2-DG-treated, non-kindled mice on day 17 compared to baseline. Only clusters with significantly different voxels are shown ($p < .05$, minimum cluster size of 10 voxels). The hot scale represents the *p* value for each voxel. For a scheme displaying location of brain regions with altered glucose intake on the used MRI template see Fig. 4E (colour code: blue, cortex; dark green, dorsal hippocampus; turquoise, ventral hippocampus; red, striatum; light green, thalamus; pink, basal ganglia; orange, amygdala; yellow, cerebellum). (For interpretation of the references to colour in this figure legend, the reader is referred to the web version of this article.)

($p = .0199$) and thalamus ($p = .0247$) of the CoKi_2-DG group compared to CoKi_vehicle at day 17 (Table 1). Raised K_i values were detected on days 10 and 17 in the CoKi_2-DG group compared to baseline in hippocampus (day 10, $p = .0017$; day 17, $p = .0005$), thalamus (day 10, $p = .0008$; day 17, p = .0002), amygdala (day 10, $p = .0040$; day 17, $p = .0009$), striatum (day 10, $p = .0195$; day 17, $p = .0050$), and cerebellum (day 10, $p = .0166$; day 17, $p = .0007$; Table 1). K_i in CoKi_2-DG mice was also higher than in the 2-DG_only group at day 10 in all analyzed brain regions (hippocampus, $p = .0191$; thalamus, $p = .0321$, amygdala, $p = .0101$; cortex, $p = .0346$; striatum, $p = .0387$; cerebellum, $p = .0330$) as well as on day 17 in amygdala ($p = .0125$; Table 1).

Regarding [^{18}F]FDG K_i, parametric *t* maps comparing CoKi_2DG and 2-DG_only animals at day 10 show that kindled mice had higher K_i values almost over the whole brain (except for some cortical areas) with particular high values in hippocampus (Fig. 3A). Compared to baseline, *t* maps show higher K_i values at 10 days in the CoKi_2-DG group in the area of basal ganglia (Fig. 3B). At day 17, this elevation became additionally evident in the hippocampus and thalamus (Fig. 3C). Accordingly, when comparing CoKi_2-DG with CoKi_vehicle, SPM analysis revealed increased glucose influx in similar regions (Fig. 3D). Parametric *t* maps of the 2-DG_only group show increased K_i values at 17 days compared to baseline primarily in the dorsal hippocampus and dorsal thalamus (Fig. 3E).

Regarding [^{18}F]FDG MR_{Glu}, parametric *t* maps revealed higher values at day 10 in the CoKi_2-DG versus 2-DG_only group restricted to the ventral hippocampus (Fig. 4A), a finding which becomes even more pronounced at day 17 (Fig. 4B). At day 17, *t* maps present higher MR_{Glu} values for CoKi_2-DG versus CoKi_vehicle mice in epilepsy-related brain regions like hippocampus and thalamus (Fig. 4C). Comparing *t* maps of 2-DG_only at day 17 with baseline higher values became obvious mainly in the dorsal hippocampus (Fig. 4A).

3.3. Immunohistochemistry

Visual inspection of GLUT1 staining did not reveal any differences between groups (not shown). Activation of microglia (IBA1) and astrocytes (GFAP) was occasionally seen in brain sections of age-matched control mice. Using semi-quantitative scoring CoKi_vehicle mice did not differ from naïve controls (Fig. 5A), while distinctly elevated microglial activation was found in the CA3a region ($p = .0030$), dentate hilus ($p = .0043$), and thalamus ($p = .0460$) of CoKi_2-DG mice (Fig. 5A,B). The CA1 region and the piriform cortex showed a tendency towards increased microglial activation ($p = .0711$ and .0521, respectively; Fig. 5A,D). In amygdala, no group differences were found (Fig. 5C). Remarkably, IBA1 staining revealed prominent microglial activation also in the 2-DG_only group in all analyzed hippocampal subregions (CA1, $p = .0076$; CA3a, $p = .0026$; dentate hilus, $p = .0015$) and the thalamus ($p = .0072$; Fig. 5A,B). Applying cell counting and morphological assessment of microglia in pre-selected areas of the previously scored brain regions, absolute numbers of microglia in kindled and/or 2-DG-treated groups did not differ from naïve mice in any region (data not shown). Morphological categorization confirmed the predominant presence of ramified microglia in naïve controls (Fig. 5A-D). In the other groups, the number of ramified microglia was lower than in controls while the number of hypertrophic microglia was increased in all analyzed subregions (Fig. 5A-C) apart from the piriform cortex in the CoKi_vehicle group (Fig. 5D). Rarely, cells of rod morphology were found (Fig. 5A). GFAP staining revealed raised astroglial activation in the CoKi_vehicle group in the CA3a region ($p = .0060$), dentate hilus ($p = .0008$), and piriform cortex ($p = .0055$), whereas in the CoKi_2-DG group this was only seen in the dentate hilus ($p = .0148$; Fig. 6A-E). 2-DG treatment alone did not lead to astroglial activation higher than in naïve controls (Fig. 6A-E). Fluoro-Jade C-positive neurons were not detected in any of the investigated groups (not shown).

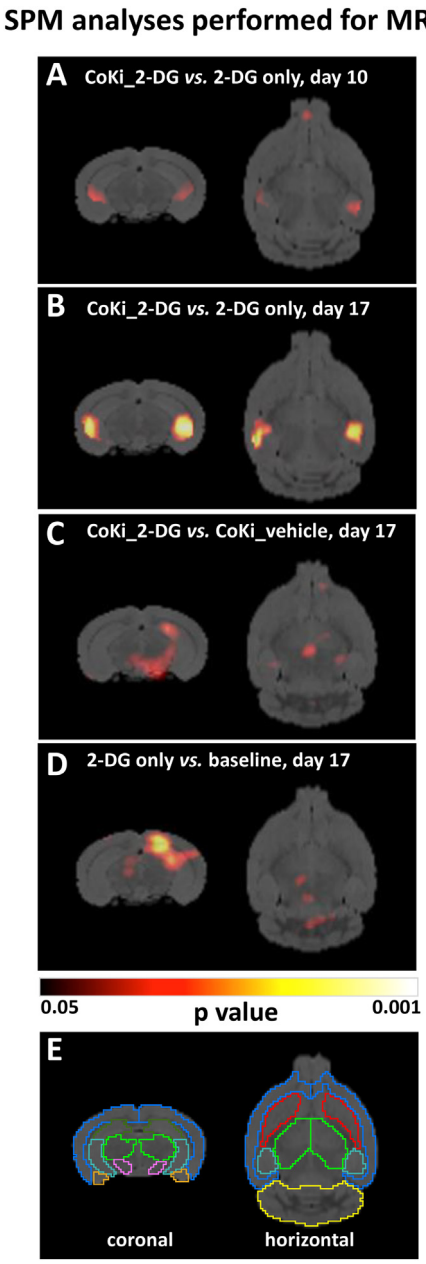

Fig. 4. Statistical parametric mapping (SPM) analysis of [^{18}F]FDG MR_{Glu} maps in mice undergoing 2-deoxy-D-glucose (2-DG) treatment in combination with or without corneal kindling (CoKi).
Coronal (~3.1 mm caudal to bregma; left), and horizontal (~1.5 mm ventral to bregma; right) *t* maps resulting from voxel wise comparisons (Student's *t*-test) of [^{18}F]FDG MR_{Glu} maps are shown for comparison of (A, B) 2-DG treated mice with and without kindling on days 10 and 17, (C) 2-DG-treated versus vehicle-treated kindled mice on day 17 compared to baseline, and (D) 2-DG treated, non-kindled mice on day 17 compared to baseline. Only clusters with significantly different voxels are shown ($p < .05$, minimum cluster size of 10 voxels). The hot scale represents the *p* value for each voxel. (E) MRI template with colour-coded labeling of brain regions which showed altered glucose intake (see Fig. 3) or turnover due to 2-DG treatment and/or kindling: Blue, cortex; dark green, dorsal hippocampus; turquoise, ventral hippocampus; red, striatum; light green, thalamus; pink, basal ganglia; orange, amygdala; yellow, cerebellum. (For interpretation of the references to colour in this figure legend, the reader is referred to the web version of this article.)

4. Discussion

Cerebral glucometabolic changes during epileptogenesis represent targets for therapeutic intervention gaining growing attention (Boison and Steinhäuser, 2017). This study was designed to evaluate potential disease-modifying effects of the glycolysis inhibitor 2-DG in the 6 Hz corneal kindling model and how this might be reflected in brain glucometabolism as assessed by translational [^{18}F]FDG PET. Our main findings are: 1. Post-stimulation treatment with 2-DG attenuates epileptogenesis and seizure severity during 6 Hz corneal kindling. 2. Repetitive 2-DG treatment alone leads to regionally increased glucose brain influx and metabolic rate at day 17 but not on day 10 or after single treatment, and, interestingly, also to microglial activation. 3. Epileptogenesis in the 6 Hz corneal kindling model in absence of glycolysis inhibition does neither alter interictal brain glucometabolism nor neuronal viability, but indeed results in prominent astroglial activation. 4. Epileptogenesis in the 6 Hz corneal kindling model in combination with post-stimulation 2-DG treatment results in elevated cerebral glucose influx and metabolic rate, as well as in microglial activation, while astroglial activation is less prominent as compared to vehicle treatment.

4.1. Disease-modifying effects of 2-DG in the 6 Hz corneal kindling model

Kindling-decelerating effects of 2-DG treatment have been shown before in rat models of kindling-mediated epileptogenesis (Garriga-Canut et al., 2006; Stafstrom et al., 2009). Notably, we here provide evidence that 2-DG treatment can impair epileptogenesis also when administered after rather than before kindling stimulations. Epileptogenesis progression during kindling, reflected by increasing seizure severity during kindling course, is based on growing susceptibility to a consistent seizure-inducing stimulus. Therefore, in kindling models a true anti-epileptogenic effect in terms of preventive activity against epileptogenesis-promoting consequences of seizures is difficult to be separated from a merely anticonvulsant action of a test compound (or a mixture of both). We aimed to account for this obstacle by choosing a treatment time point of 1 min after each stimulation, hereby minimizing a direct anticonvulsant action of 2-DG as far as possible. To our knowledge, pharmacokinetic data for 2-DG in mice are not available in the literature, but pharmacokinetics of 2-DG have been studied in humans and rats reporting elimination half-lifes of about 3 to 5 h (Gounder et al., 2012; Raez et al., 2013; Umegae et al., 1990). Assuming a similar pharmacokinetic profile of 2-DG in mice and considering a reported peak of its anticonvulsant action against 6 Hz seizures in mice at 1 h post administration (Stafstrom et al., 2009), it seems unlikely that 2-DG should still exert a distinct direct anticonvulsant effect on the next stimulation, which was applied at least 6 h later.

4.2. Effects of 2-DG treatment and kindling on cerebral glucometabolism

To the best of our knowledge, impact of chronic 2-DG treatment as well as kindling-mediated epileptogenesis on cerebral glucose metabolism in mice has not been evaluated before. Here, we applied [^{18}F]FDG PET, which represents a reliable and translational in vivo method to examine brain glucose metabolism (Goffin et al., 2008; O'Brien and Jupp, 2009). Like glucose, [^{18}F]FDG is transported across the BBB via GLUT1, and then taken up by brain cells again via glucose transporters. Intracellular phosphorylation prevents [^{18}F]FDG from being released again. This metabolic trapping and subsequent radioactive decay represents a good marker for glucose uptake and turnover. Here, chronic 2-DG treatment per se resulted in raised brain glucose influx and metabolic rate. Maximum K_i and MR_{Glu} values were reached only on day 17, suggesting that duration of 2-DG treatment determines the extent of glucometabolic alterations in the healthy brain. In the brain undergoing kindling-mediated epileptogenesis (CoKi_vehicle), [^{18}F]FDG PET did

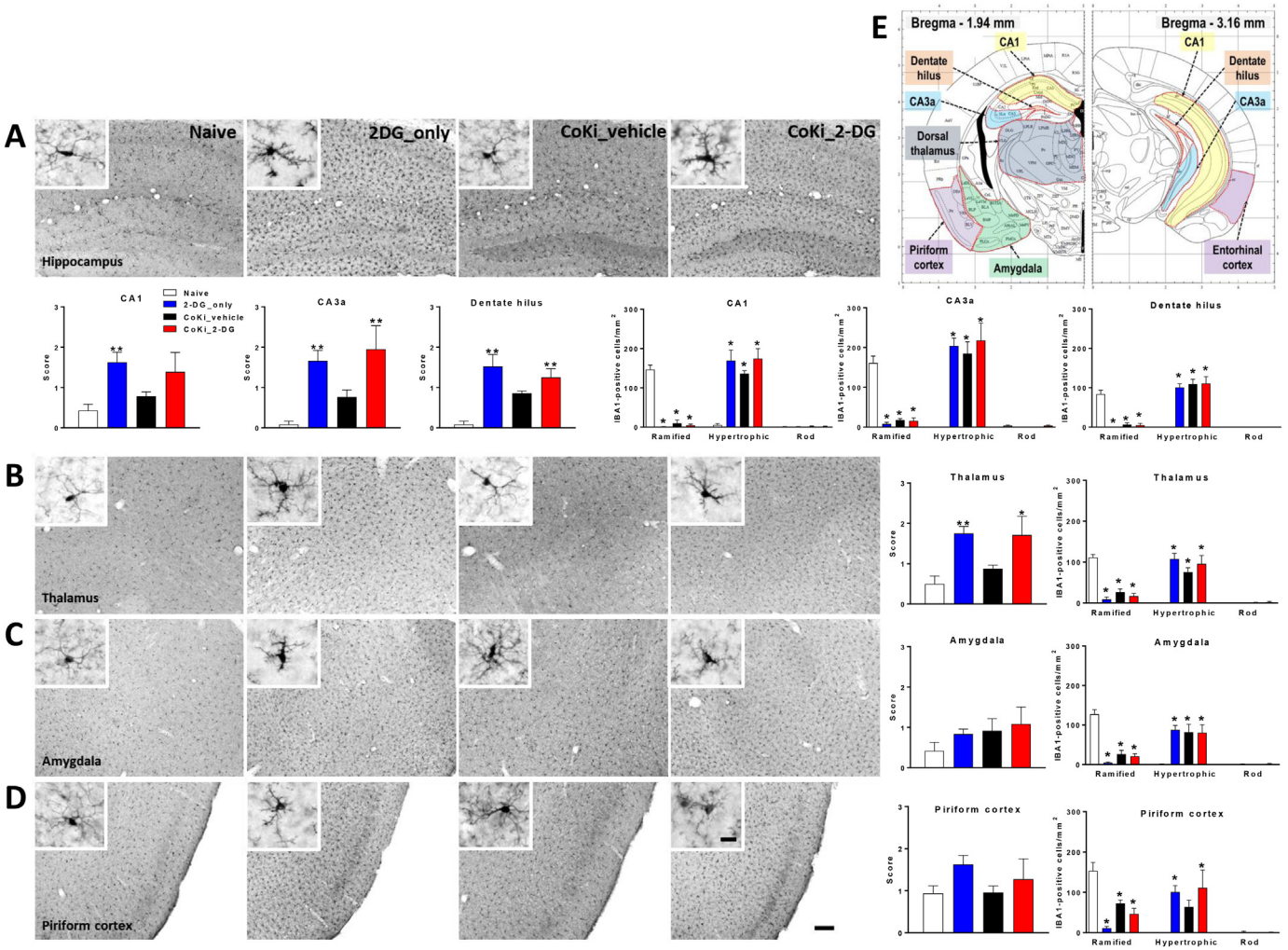

Fig. 5. Results of immunohistological microglia activation analysis.
Images of (A) the right hippocampal area, (B) the thalamus, (C) the amygdala, and (D) the piriform cortex showing IBA1-positive microglia being representative for morphological subtypes observed in analyzed brain regions of the respective experimental group at day 22 after start of experiment. Data of semi-quantitative assessment of microglial activation as well as quantitative morphological subtype analysis of IBA1-positive cells in the analyzed brain regions is illustrated (A) below or (B-D) beside the respective images. Details on analysis methods are provided in the methods section. (E) Scheme displaying the brain regions analyzed (modified from Paxinos and Franklin, 2001; *permission for reprint has been requested*). Naïve (untreated, unstimulated) control group, $n = 6$; 2-DG_only, 2-deoxy-D-glucose-treated, unstimulated mice, $n = 6$; CoKi_vehicle, vehicle-treated mice undergoing kindling, $n = 6$; CoKi_2-DG, 2-DG- treated mice undergoing kindling, $n = 6$; CA, cornu ammonis. Mean ± SEM; Kruskal-Wallis ANOVA, Dunn's multiple comparison post hoc test for semiquantitative scoring or ordinary one-way ANOVA, Dunnett's multiple comparisons post hoc test for quantitative morphological subtype analysis, respectively; $p < .05$. Asterisk indicates significant difference to naïve control group. Bar in (A) indicates 75 µm and 10 µm (magnified detail), respectively.

not identify altered brain glucose supply or turnover (Table 1), neither during nor at the end of epileptogenesis, which corresponds to results of a [^{14}C]2-DG autoradiography study in a rat rapid kindling model (Lothman et al., 1985). One could expect both hypo- and hypermetabolic changes induced by the kindling process. While glucose hypometabolism might result from neuronal death or endogenous anti-epileptic/epileptogenic mechanisms occurring post seizure exhibition, like increase in GABAergic inhibition and reduced (excitatory) neuronal activity, hypermetabolism might be a consequence of epileptogenesis-triggered neuronal and/or astrocytic activation. One explanation for not finding changes in glucose metabolism during kindling progression could be that we performed PET interictally. This was done to rule out detecting increased [^{18}F]FDG uptake as a merely result of convulsions (Blackwood et al., 1981) instead of imaging energy-demanding processes associated with epileptogenesis itself. In the interictal phase during epileptogenesis in the 6 Hz kindling model, however, potentially decreased or increased neuronal and astroglial activation might not be pronounced enough to be detected by [^{18}F]FDG PET against the background glucose turnover. Supporting this idea, a recently published study using pentylentetrazole-mediated kindling in rats, which is accompanied by neurodegeneration indeed (Park et al., 2006), found reduced [^{18}F]FDG uptake in the hippocampus being predictive for positive kindling response (Bascunana et al., 2016). We here report that 6 Hz corneal kindling over 21 days does not lead to neurodegeneration, which is in line with data from the 50 Hz corneal kindling model (Loewen et al., 2016). This lack of distinct neurodegeneration might explain why hypometabolism was also not detected in fully-kindled mice. In addition, continuous anaesthesia is needed for acquiring dynamic PET data which is also known to influence brain glucometabolism (Toyama et al., 2004). Lastly, hypo- and hypermetabolic changes might also occur simultaneously and level each other out. Interestingly, our data suggest that kindling and 2-DG synergistically enhance glucose influx, especially during kindling progression (day 10; Table 1). Neuronal firing due to seizing leads to a higher energy demand, and therefore also uptake of [^{18}F]FDG is expected to increase. Compensatory elevation of brain energy supply will have to be even higher under

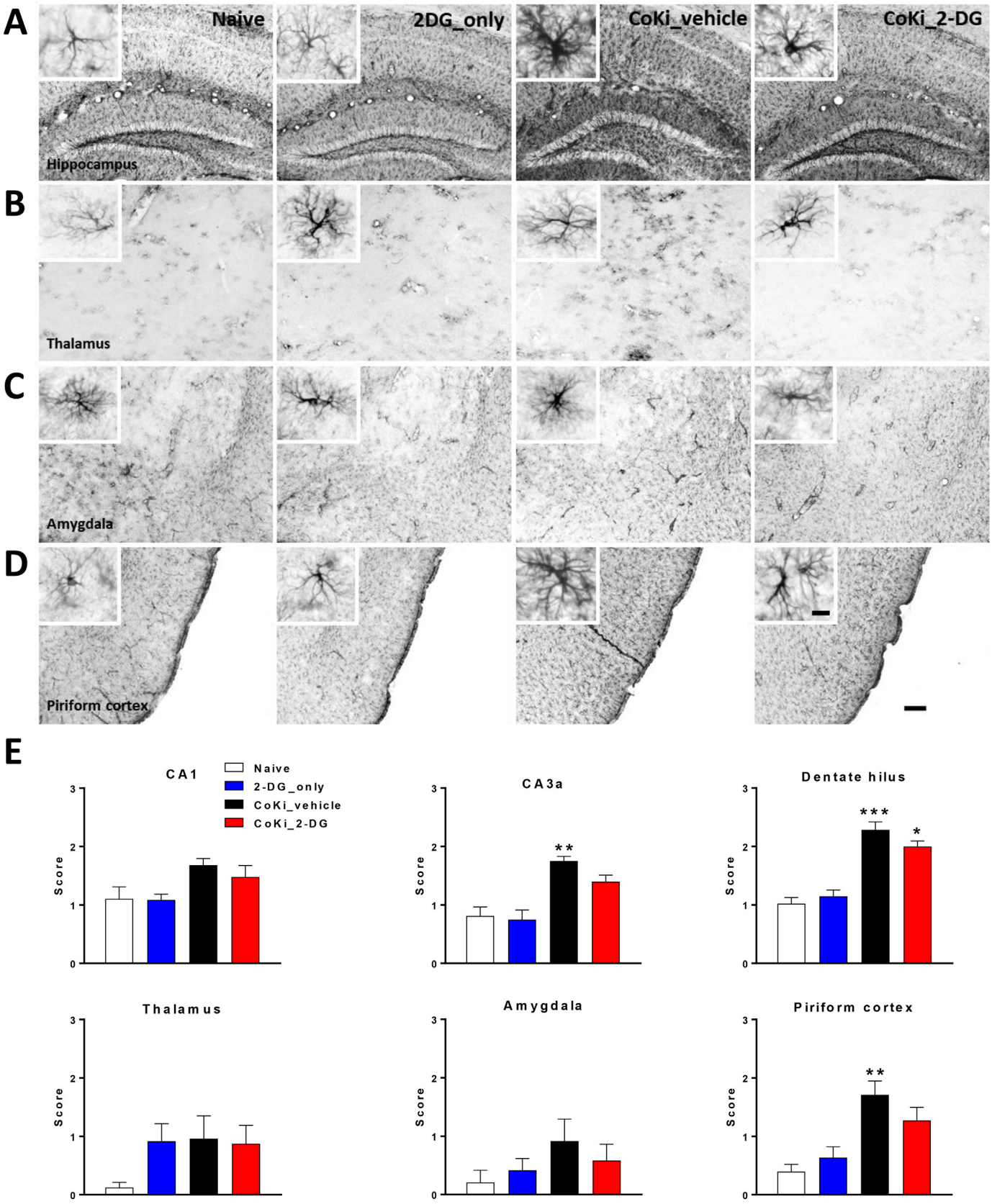

Fig. 6. Results of immunohistological astroglia activation analysis.
Representative images of (A) the right hippocampal area, (B) the thalamus, (C) the amygdala, and (D) the piriform cortex showing GFAP-positive astroglia of each experimental group at day 22 after start of experiment. (E) Data of semi-quantitative assessment of astroglial activation in hippocampal subregions, thalamus, amygdala and piriform cortex. Mean ± SEM; Kruskal-Wallis ANOVA, Dunn's multiple comparison post hoc test; $p < .05$. Asterisk indicates significant difference to naïve control group. Bar in (D) indicates 75 µm and 10 µm (magnified detail), respectively. For details about treatment groups and abbreviations see legend of Fig. 5.

an energetic stress situation like impaired glucose utilization mediated here by simultaneous 2-DG treatment. The combined effect of 2-DG and kindling was also reflected by an increase in MR_{Glu} at day 17 in hippocampus and thalamus, i.e. in brain regions relevant for seizure origin and spread, whose neurons might be especially energy demanding due to seizure responses of increasing severity during the kindling course. Moreover, kindling-induced seizures will lead to increased glutamate release. It has been suggested that astrocytic activation by glutamate results in a decreased glucose utilization in neurons but increased glycolysis by astrocytes leading to lactate production which is then exported through the so-called astrocyte-neuron-lactate-shuttle to fuel the neuronal citric acid cycle (Magistretti and Allaman, 2015). Increased astrocytic glucose metabolism might be all the more pronounced in the presence of 2-DG hampering glycolysis. The increased energy demand may also promote glycogenolysis in astrocytes, being the only cells in the brain that store glycogen (Magistretti and Allaman, 2015), which would additionally add to elevated glucose metabolism. Indeed, we here also discovered kindling-mediated astroglial activation in several limbic brain regions by immunohistological analysis, which is in agreement with recent findings in the 50 Hz corneal kindling model (Loewen et al., 2016). The elevated energy demand of neurons and activated astrocytes during kindling progression might have been met through the observed elevation in brain glucose supply and in consequence have ameliorated the kindling process.

The brain atlas-independent SPM analysis substantiates the findings of kinetic modelling by revealing increased glucose influx in major parts of the brain with a hot spot in the hippocampus (Fig. 3E) when comparing the CoKi_2-DG with 2-DG_only on day 10. This finding argues for involvement of the whole brain into the kindling process, but the magnitude of affection is apparently prominent in typically epilepsy-related areas. Interestingly, SPM analysis of MR_{Glu} demonstrates elevated glucose turnover in the CoKi_2-DG group limited to epilepsy-associated brain regions (hippocampus, thalamus; Fig. 4B-D), which were also affected by astroglial and microglial activation in histological investigations. This increase in hippocampal glucose metabolism became more pronounced after 17 days of kindling and therefore seems to be influenced by the duration of epileptogenesis under energy restriction. Furthermore, the duration of energy restriction might have caused profound cellular changes in energy utilization. MR_{Glu} parametric maps might reflect pronounced compensatory upregulation of glycolysis / lactate production by activated astrocytes to meet the epileptogenesis-associated increased energy demand of activated hippocampal and thalamic neurons.

4.3. Effects of kindling and 2-DG treatment on constituents of the neurovascular unit and blood glucose

To assess whether the observed increased glucose influx could be explained by an altered expression of GLUT1 transporters, being responsible for glucose brain uptake across the BBB as well as glucose uptake by astrocytes we performed immunohistological analysis of GLUT1 expression at day 22 of kindling. Increased expression and transport activity of the 55-kDa GLUT1 due to chronic hypoglycaemia have been described before, whereas chronic hyperglycemia had no impact (Simpson et al., 1999). In our study, 2-DG led to mildly reduced blood glucose values at day 17 of 2-DG treatment in mice undergoing kindling (Fig. 2F). However, immunohistochemical staining did not reveal any obvious influence of kindling or 2-DG treatment, or the combination of both, on GLUT1 expression. It might therefore be, that more pronounced hypoglycemia is necessary to increase GLUT1 expression at the BBB. As the Fluoro-Jade-C staining did not reveal dying neurons, positive effects of 2-DG on corneal kindling progress cannot be attributed to a possible neuroprotective action. Rather, astroglial activation was not as prominent in the hippocampal CA3 region and the piriform cortex of 2-DG-treated mice that underwent kindling. As seizure-triggered glutamate release can lead to astrocytic activation, one may argue that this alleviation could be due to less exhibited seizures in the 2-DG treated group until the end of kindling when brains were harvested. However, mice whose brains were randomly chosen for histological analyses did not differ in the number of experienced generalized seizures during kindling course (33.50 vs. 30.50, CoKi_vehicle vs. CoKi_2-DG, median, Mann Whitney test, $p = .1234$). The less prominent astrocyte activation in 2-DG-treated mice might be a result of the 2-DG-triggered increased energy supply enabling astrocytes to encounter some of epileptogenesis-induced alterations, including higher neuronal energy demand. IBA1 staining revealed only limited microglial activation induced by kindling compared to brain slices of naïve control mice (Fig. 5), which is generally in line with data from 50-Hz-kindled mice (Loewen et al., 2016). IBA1 is a protein specifically expressed in monocytic cell lines (Imai et al., 1996) and increased in activated macrophages/microglia (Ito et al., 1998). Surprisingly, however, we found that 2-DG led to strong microglial activation both in unstimulated mice and in mice undergoing kindling. Cumulating evidence suggests that microglial activation plays a crucial role in epileptogenesis (Amhaoul et al., 2015; Brackhan et al., 2016; Vezzani, 2015). Due to their continuous patrolling tasks for maintaining a healthy microenvironment for neuronal survival in the CNS, microglia require huge energy sources including glucose (Kalsbeek et al., 2016). Microglial activation by 2-DG and epileptogenesis will probably lead to even higher energy demands compensated by elevated glucose utilization. Therefore, the increased glucose turnover detected here by [^{18}F]FDG PET in the 2-DG treated mice might partially also reflect increased microglial glucose consumption. Immunostaining with IBA1 is not suitable for differentiation of the pro-inflammatory M1 and the anti-inflammatory M2 state. Therefore, it remains to be elucidated in future investigations whether 2-DG might preferentially induce the reparative anti-inflammatory M2 phenotype and whether this might contribute to the disease-modifying effects of 2-DG found in the present study.

5. Conclusion

In conclusion, we show that chronic 2-DG treatment in mice is well tolerated and exerts disease-modifying effects in the 6 Hz kindling model of difficult-to-treat seizures. As revealed by [^{18}F]FDG PET, 2-DG leads to increased glucose supply both in the healthy mouse brain and in the mouse brain undergoing kindling-mediated epileptogenesis. Together with the alleviated astrocytosis and the activation of microglia by 2-DG this might contribute to the positive interference with epileptogenesis.

Acknowledgements

This work was supported by the European Union Seventh's Framework Programme (FP7/2007-2013) under grant agreement n°602102 (EPITARGET). Ina Leiter was supported by a scholarship from the Konrad-Adenauer-Stiftung e.V.. We are grateful to Silvia Eilert, Petra Felsch, Alexander Kanwischer, Dr. Tobias Ross, Simone Mehler, Michael Weißing, Lena Schrey, Nathalie Hildebrandt, and Annika Thomer for excellent technical assistance. Dr. Wolfgang Härtig is kindly acknowledged for help with immunohistochemical staining. We thank Dr. Helge Frieling for providing the stimulator used for corneal kindling.

Declaration of Competing Interest

None.

References

Amhaoul, H., Hamaide, J., Bertoglio, D., Reichel, S.N., Verhaeghe, J., Geerts, E., et al., 2015. Brain inflammation in a chronic epilepsy model: evolving pattern of the translocator protein during epileptogenesis. Neurobiol. Dis. 82, 526–539.

Bascunana, P., Javela, J., Delgado, M., Fernandez de la Rosa, R., Shiha, A.A., Garcia-Garcia, L., et al., 2016. [(18)F]FDG PET neuroimaging predicts pentylenetetrazole (PTZ) kindling outcome in rats. Mol. Imaging Biol. 18 (5), 733–740.
Baulac, M., de Boer, H., Elger, C., Glynn, M., Kalviainen, R., Little, A., et al., 2015. Epilepsy priorities in Europe: a report of the ILAE-IBE epilepsy advocacy Europe Task Force. Epilepsia 56 (11), 1687–1695.
Bialer, M., Johannessen, S.I., Levy, R.H., Perucca, E., Tomson, T., White, H.S., 2017. Progress report on new antiepileptic drugs: a summary of the thirteenth Eilat conference on new antiepileptic drugs and devices (EILAT XIII). Epilepsia 58 (2), 181–221.
Blackwood, D.H., Kapoor, V., Martin, M.J., 1981. Regional changes in cerebral glucose utilization associated with amygdaloid kindling and electroshock in the rat. Brain Res. 224 (1), 204–208.
Boison, D., Steinhäuser, C., 2017. Epilepsy and astrocyte energy metabolism. Glia 66 (6), 1235–1243.
Brackhan, M., Bascunana, P., Postema, J.M., Ross, T.L., Bengel, F.M., Bankstahl, M., et al., 2016. Serial quantitative TSPO-targeted PET reveals peak microglial activation up to 2 weeks after an epileptogenic brain insult. J. Nucl. Med. 57 (8), 1302–1308.
Burneo, J.G., Poon, R., Kellett, S., Snead, O.C., 2015. The utility of positron emission tomography in epilepsy. Can. J. Neurol. Sci. (6), 1–12.
Chen, W., Gueron, M., 1992. The inhibition of bovine heart hexokinase by 2-deoxy-D-glucose-6-phosphate: characterization by 31P NMR and metabolic implications. Biochimie 74 (9–10), 867–873.
Drzezga, A., Arnold, S., Minoshima, S., Noachtar, S., Szecsi, J., Winkler, P., et al., 1999. 18F-FDG PET studies in patients with extratemporal and temporal epilepsy: evaluation of an observer-independent analysis. J. Nucl. Med. 40 (5), 737–746.
Garriga-Canut, M., Schoenike, B., Qazi, R., Bergendahl, K., Daley, T.J., Pfender, R.M., et al., 2006. 2-deoxy-D-glucose reduces epilepsy progression by NRSF-CtBP-dependent metabolic regulation of chromatin structure. Nat. Neurosci. 9 (11), 1382–1387.
Gasior, M., Yankura, J., Hartman, A.L., French, A., Rogawski, M.A., 2010. Anticonvulsant and proconvulsant actions of 2-deoxy-D-glucose. Epilepsia 51 (8), 1385–1394.
Goffin, K., Dedeurwaerdere, S., Van Laere, K., Van Paesschen, W., 2008. Neuronuclear assessment of patients with epilepsy. Semin. Nucl. Med. 38 (4), 227–239.
Goffin, K., Van Paesschen, W., Dupont, P., Van Laere, K., 2009. Longitudinal microPET imaging of brain glucose metabolism in rat lithium-pilocarpine model of epilepsy. Exp. Neurol. 217 (1), 205–209.
Gounder, M.K., Lin, H., Stein, M., Goodin, S., Bertino, J.R., Kong, A.N., et al., 2012. A validated bioanalytical HPLC method for pharmacokinetic evaluation of 2-deoxyglucose in human plasma. Biomed. Chromatogr. 26 (5), 650–654.
Gröticke, I., Hoffmann, K., Löscher, W., 2007. Behavioral alterations in the pilocarpine model of temporal lobe epilepsy in mice. Exp. Neurol. 207 (2), 329–349.
Imai, Y., Ibata, I., Ito, D., Ohsawa, K., Kohsaka, S., 1996. A novel gene iba1in the major histocompatibility complex class III region encoding an EF hand protein expressed in a monocytic lineage. Biochem. Biophys. Res. Commun. 224 (3), 855–862.
Ito, D., Imai, Y., Ohsawa, K., Nakajima, K., Fukuuchi, Y., Kohsaka, S., 1998. Microglia-specific localisation of a novel calcium binding protein, Iba1. Mol. Brain Res. 57 (1), 1–9.
Jupp, B., Williams, J., Binns, D., Hicks, R.J., Cardamone, L., Jones, N., et al., 2012. Hypometabolism precedes limbic atrophy and spontaneous recurrent seizures in a rat model of TLE. Epilepsia 53 (7), 1233–1244.
Kalsbeek, M.J., Mulder, L., Yi, C.X., 2016. Microglia energy metabolism in metabolic disorder. Mol. Cell. Endocrinol. 438, 27–35.
Kilkenny, C., Browne, W.J., Cuthill, I.C., Emerson, M., Altman, D.G., 2010. Improving bioscience research reporting: the ARRIVE guidelines for reporting animal research. PLoS Biol. 8 (6), e1000412.
Kipnis, D.M., Cori, C.F., 1959. Studies of tissue permeability. V. The penetration and phosphorylation of 2-deoxyglucose in the rat diaphragm. J. Biol. Chem. 234 (1), 171–177.
Kornblum, H.I., Araujo, D.M., Annala, A.J., Tatsukawa, K.J., Phelps, M.E., Cherry, S.R., 2000. In vivo imaging of neuronal activation and plasticity in the rat brain by high resolution positron emission tomography (microPET). Nat. Biotechnol. 18 (6), 655–660.
Lanz, B., Poitry-Yamate, C., Gruetter, R., 2014. Image-derived input function from the vena cava for 18F-FDG PET studies in rats and mice. J. Nucl. Med. 55 (8), 1380–1388.
Leclercq, K., Matagne, A., Kaminski, R.M., 2014. Low potency and limited efficacy of antiepileptic drugs in the mouse 6Hz corneal kindling model. Epilepsy Res. 108 (4), 675–683.
Lee, E.M., Park, G.Y., Im, K.C., Kim, S.T., Woo, C.W., Chung, J.H., et al., 2012. Changes in glucose metabolism and metabolites during the epileptogenic process in the lithium-pilocarpine model of epilepsy. Epilepsia 53 (5), 860–869.
Lian, X.Y., Khan, F.A., Stringer, J.L., 2007. Fructose-1,6-bisphosphate has anticonvulsant activity in models of acute seizures in adult rats. J. Neurosci. 27 (44), 12007–12011.
Liu, Y.R., Cardamone, L., Hogan, R.E., Gregoire, M.C., Williams, J.P., Hicks, R.J., et al., 2010. Progressive metabolic and structural cerebral perturbations after traumatic brain injury: an in vivo imaging study in the rat. J. Nucl. Med. 51 (11), 1788–1795.
Loewen, J.L., Barker-Haliski, M.L., Dahle, E.J., White, H.S., Wilcox, K.S., 2016. Neuronal injury, gliosis, and glial proliferation in two models of temporal lobe epilepsy. J. Neuropathol. Exp. Neurol. 75 (4), 366–378.
Löscher, W., Brandt, C., 2010. Prevention or modification of epileptogenesis after brain insults: experimental approaches and translational research. Pharmacol. Rev. 62 (4), 668–700.
Lothman, E.W., Hatlelid, J.M., Zorumski, C.F., 1985. Functional mapping of limbic seizures originating in the hippocampus: a combined 2-deoxyglucose and electrophysiologic study. Brain Res. 360 (1–2), 92–100.
Ma, Y., Hof, P.R., Grant, S.C., Blackband, S.J., Bennett, R., Slatest, L., et al., 2005. A three-dimensional digital atlas database of the adult C57BL/6J mouse brain by magnetic resonance microscopy. Neuroscience 135 (4), 1203–1215.
Magistretti, P.J., Allaman, I., 2015. A cellular perspective on brain energy metabolism and functional imaging. Neuron 86 (4), 883–901.
Mirrione, M.M., Schiffer, W.K., Siddiq, M., Dewey, S.L., Tsirka, S.E., 2006. PET imaging of glucose metabolism in a mouse model of temporal lobe epilepsy. Synapse 59 (2), 119–121.
Mirrione, M.M., Schiffer, W.K., Fowler, J.S., Alexoff, D.L., Dewey, S.L., Tsirka, S.E., 2007. A novel approach for imaging brain-behavior relationships in mice reveals unexpected metabolic patterns during seizures in the absence of tissue plasminogen activator. NeuroImage 38 (1), 34–42.
Nirenberg, M.W., Hogg, J.F., 1958. Inhibition of anaerobic glycolysis in Ehrlich ascites tumor cells by 2-deoxy-D-glucose. Cancer Res. 18 (5), 518–521.
O'Brien, T.J., Jupp, B., 2009. In-vivo imaging with small animal FDG-PET: a tool to unlock the secrets of epileptogenesis? Exp. Neurol. 220 (1), 1–4.
Park, J.H., Cho, H., Kim, H., Kim, K., 2006. Repeated brief epileptic seizures by pentylenetetrazole cause neurodegeneration and promote neurogenesis in discrete brain regions of freely moving adult rats. Neuroscience 140 (2), 673–684.
Paxinos, G., Franklin, K.B.J., 2001. The Mouse Brain in Stereotaxic Coordinates, 2nd edn. Academic Press, San Diego.
Racine, R.J., 1972. Modification of seizure activity by electrical stimulation: II. Motor seizure. Electroencephalogr. Clin. Neurophysiol. 32 (3), 281–294.
Raez, L.E., Papadopoulos, K., Ricart, A.D., Chiorean, E.G., Dipaola, R.S., Stein, M.N., et al., 2013. A phase I dose-escalation trial of 2-deoxy-D-glucose alone or combined with docetaxel in patients with advanced solid tumors. Cancer Chemother. Pharmacol. 71 (2), 523–530.
Simpson, I.A., Appel, N.M., Hokari, M., Oki, J., Holman, G.D., Maher, F., et al., 1999. Blood-brain barrier glucose transporter: effects of hypo- and hyperglycemia revisited. J. Neurochem. 72 (1), 238–247.
Stafstrom, C.E., Roopra, A., Sutula, T.P., 2008. Seizure suppression via glycolysis inhibition with 2-deoxy-D-glucose (2DG). Epilepsia 8, 97–100.
Stafstrom, C.E., Ockuly, J.C., Murphree, L., Valley, M.T., Roopra, A., Sutula, T.P., 2009. Anticonvulsant and antiepileptic actions of 2-deoxy-D-glucose in epilepsy models. Ann. Neurol. 65 (4), 435–447.
Struck, A.F., Westover, M.B., Hall, L.T., Deck, G.M., Cole, A.J., Rosenthal, E.S., 2016. Metabolic correlates of the ictal-interictal continuum: FDG-PET during continuous EEG. Neurocrit. Care. 24 (3), 324–331.
Thorn, S.L., deKemp, R.A., Dumouchel, T., Klein, R., Renaud, J.M., Wells, R.G., et al., 2013. Repeatable noninvasive measurement of mouse myocardial glucose uptake with 18F-FDG: evaluation of tracer kinetics in a type 1 diabetes model. J. Nucl. Med. 54 (9), 1637–1644.
Toyama, H., Ichise, M., Liow, J.S., Vines, D.C., Seneca, N.M., Modell, K.J., et al., 2004. Evaluation of anesthesia effects on [18F]FDG uptake in mouse brain and heart using small animal PET. Nucl. Med. Biol. 31 (2), 251–256.
Umegae, Y., Nohta, H., Ohkura, Y., 1990. Simultaneous determination of 2-deoxy-D-glucose and D-glucose in rat serum by high-performance liquid chromatography with post-column fluorescence derivatization. Chem. Pharm. Bull. 38 (4), 963–965.
Vezzani, A., 2015. Anti-inflammatory drugs in epilepsy: does it impact epileptogenesis? Expert Opin. Drug Saf. 14 (4), 583–592.
WHO, 2018. World Health Organization Fact Sheets Epilepsy.
Wick, A.N., Drury, D.R., Nakada, H.I., Wolfe, J.B., 1957. Localization of the primary metabolic block produced by 2-deoxyglucose. J. Biol. Chem. 224 (2), 963–969.
Wyatt-Johnson, S.K., Herr, S.A., Brewster, A.L., 2017. Status epilepticus triggers time-dependent alterations in microglia abundance and morphological phenotypes in the Hippocampus. Front. Neurol. 8, 700.
Xi, H., Kurtoglu, M., Lampidis, T.J., 2014. The wonders of 2-deoxy-D-glucose. IUBMB Life 66 (2), 110–121.
Yang, H., Guo, R., Wu, J.X., Peng, Y.F., Xie, D.J., Zheng, W., et al., 2013. The antiepileptic effect of the glycolytic inhibitor 2-deoxy-d-glucose is mediated by upregulation of K-ATP channel subunits Kir6.1 and Kir6.2. Neurochem. Res. 38 (4), 677–685.
Zhang, L., Guo, Y., Hu, H., Wang, J., Liu, Z., Gao, F., 2015. FDG-PET and NeuN-GFAP immunohistochemistry of hippocampus at different phases of the pilocarpine model of temporal lobe epilepsy. Int. J. Med. Sci. 12 (3), 288–294.